A continuous approach to the aeroelastic stability of suspended cables in 1:2 internal resonance

Angelo Luongo, Giuseppe Piccardo

A Continuous Approach to the Aeroelastic Stability of Suspended Cables in 1 : 2 Internal Resonance

A. LUONGO
Dipartimento di Ingegneria delle Strutture, delle Acque e del Terreno, University of L'Aquila, 67040 Monteluco di Roio, L'Aquila, Italy (luongo@ing.univaq.it)

G. PICCARDO
Dipartimento di Ingegneria delle Costruzioni, dell'Ambiente e del Territorio, University of Genoa, Via Montallegro 1, 16145 Genoa, Italy

(Received 3 February 2006; accepted 10 August 2006)

Abstract: This paper proposes a continuous perturbation treatment of the nonlinear equations of a cable, which is characterized by possible aeroelastic instability and internal resonance conditions. The objective is to evaluate the influence of stable modes (called passive) usually ignored when discretizing the model. The first step concerns the description of the structural equilibrium path under the action of the mean wind forces. Then, a multiple scale perturbation analysis of the integro-differential equations of motion is performed. Analyzing the stability of the reduced system, the existence of some limit cycles and of successive bifurcations is investigated. The comparison with previous papers, developed in the discrete field, allows clarification of the actual influence of the static equilibrium path and the contribution of passive modes.

Keywords: Galloping, cable dynamics, aeroelasticity, bifurcation

1. INTRODUCTION

Iced cables subjected to wind action can experience a phenomenon of aeroelastic instability, called galloping, which occurs at relatively low wind speed. Galloping manifests itself by oscillations of great amplitude, which become stable on limit cycles or are divergent over time, according to the nonlinear characteristics of the system. The phenomenon is generally well described by a single degree-of-freedom (dof) model (called active dof), that can be derived from a sectional model (e.g. Blevins, 1990) or deduced by the discretization of a continuous model (e.g. Novak, 1969). Indeed, the ignored stable modes (called passive) often give a marginal contribution to the motion; for this reason the instability shape is called mono-modal galloping. However, if the natural frequencies of the mechanical model are in integer ratios $1:1$, $1:2$, ..., that is if the system is in internal resonance conditions, more modes can be involved in the motion. Because of the strong modal coupling due to resonance, the unstable motion significantly excites the stable modes, thus originating multi-modal galloping.

The problem has been studied by the authors in the linear field, with a two-dof sectional model in $1:1$ internal resonance (Luongo and Piccardo, 2005), and in the nonlinear

field, referring to a two-dof model obtained by discretizing the continuous equations of a sagged cable in 1 : 2 internal resonance (Luongo and Piccardo, 1998). In particular, in the latter paper, a cable is considered having the first symmetric in-plane frequency double with regard to the first symmetric out-of-plane frequency (first cross-over point), and the quasi-steady theory is used to deduce the aerodynamic forcing terms (e.g. Piccardo, 1993). The fluid-mechanical model thus obtained has been discretized through the two resonant eigenfunctions; a detailed analysis of the system post-critical behaviour has been carried out using a perturbation approach. Among other things, this study has highlighted the importance of the wind mean force, which modifies the equilibrium position of the cable and, consequently, the initial mechanical properties. This topic has recently been addressed by Martinelli and Perotti (2004) through a numerical approach using the finite element method.

The present paper proposes a refinement of the analysis carried out by Luongo and Piccardo (1998), consisting in a more accurate and simpler description of the equilibrium configuration of an elastic sagged cable, and in a direct perturbation treatment in the continuous field, similarly to some papers dealing with cable vibrations (Pakdemirli *et al*., 1995; Rega *et al*., 1999; Lacarbonara *et al*., 2005). The structural equilibrium path under the action of the mean wind force is first described. By assuming a uniform distribution of forces, the cable lies on an inclined plane whose angle with the vertical is a function of the wind mean velocity. The equations governing the motion around this equilibrium position are formally identical to the cable equations with the sole self-weight, except for the use of a fictitious gravity force that depends on the wind mean speed. Then, a multiple-scale perturbation analysis of the integro-differential equations of motion is carried out. The two resonant modes, whose amplitudes are unknown functions of slow time scales, are selected as generating solution. The modifications of the oscillation spatial shape are then determined. They are mainly induced by quadratic mechanical nonlinearities and can be significant, as recently discussed in the literature (e.g. Steindl and Troger, 2001). By imposing solvability conditions of the perturbation equations at different orders, and reconstituting them in a suitable way, a reduced system of three ordinary differential equations in time is obtained (called *modulation* or *bifurcation equations*). They rule the temporal evolution of the unknown amplitudes and of the phase difference of the two resonant modes. The reduced system is asymptotically equivalent to the original continuous system, and it is able to describe its essential aspects. Through the usual techniques of the Theory of Dynamic Systems a stability analysis of the reduced system is carried out in order to investigate the existence of limit cycles (periodic solutions) and successive bifurcations.

2. THE MODEL

Let us consider a cable as an elastic mono-dimensional continuum of Cauchy, subjected to its dead weight, to inertial and viscous forces, and to aerodynamic actions driven by an air fluid flow of mean velocity $\mathbf{U}$, with $U = \|\mathbf{U}\|$. The following configurations can be distinguished (Figure 1): (a) the initial configuration of equilibrium $\mathcal{C}_0$, where the cable is subjected solely to the self-weight $-mg\mathbf{a}_y$ (Figure 1(a)); (b) the reference configuration $\overline{\mathcal{C}}$, where the cable is subjected to the dead weight and to the steady component $\overline{\mathbf{b}}_a$ of the aerodynamic force $\mathbf{b}_a$ (Figure 1(b)); (c) the actual configuration $\mathcal{C}$, which is a function of the time t, where the cable is also subjected to the non-steady component $\widehat{\mathbf{b}}_a := \mathbf{b}_a - \overline{\mathbf{b}}_a$ of the aerodynamic force,

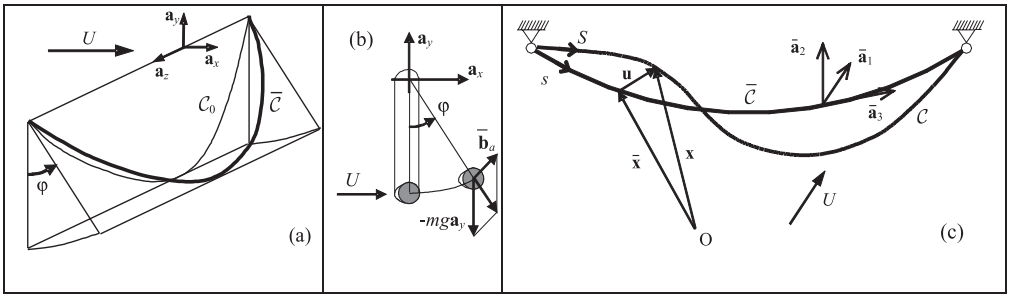

Figure 1. (a) Initial and reference configuration; (b) forces in the reference configuration; (c) present configuration.

as well as to inertial and viscous forces (Figure 1(c)). The configuration $\mathcal{C}_0$ lies on a vertical plane. The configuration $\overline{\mathcal{C}}$ is assumed planar too, supposing that the binormal component $\bar{b}_{a1} = \bar{\mathbf{b}}_a \cdot \bar{\mathbf{a}}_1$ of the steady aerodynamic force is constant along the cable. Calling φ the angle that the plane containing $\overline{\mathcal{C}}$ sets up with the vertical, equilibrium requires that

$$mg \sin\varphi - \bar{b}_{a1}(\varphi, U) = 0 \tag{1}$$

from which it is possible to deduce the equilibrium path $\varphi = \varphi(U)$. The aim is to describe the motion in a small, but finite, neighbourhood of $\overline{\mathcal{C}}$.

2.1. The mechanical model

By referring all the quantities to the reference configuration $\overline{\mathcal{C}}$, the motion of the cable is governed by the following equations:

$$\begin{aligned} &(\mathbf{t} - \bar{\mathbf{t}})' + \hat{\mathbf{b}} - m\ddot{\mathbf{x}} = \mathbf{0} \\ &\varepsilon = (\mathbf{x}' \cdot \mathbf{x}')^{1/2} - 1 \\ &\mathbf{t} = \frac{T}{1+\varepsilon}\mathbf{x}', \quad T = \bar{T} + EA\varepsilon. \end{aligned} \tag{2}$$

The first equation (2) is the incremental equilibrium equation, where $\mathbf{t}$ is the tension in the actual configuration $\mathcal{C}$, $\bar{\mathbf{t}}$ is the tension in $\overline{\mathcal{C}}$, $\hat{\mathbf{b}} := \hat{\mathbf{b}}_a + \hat{\mathbf{b}}_v$ is the specific incremental force of volume, comprehensive of the aerodynamic and viscous forces; $\mathbf{x}$ is the position occupied by the generic material point in $\mathcal{C}$; the apex and the dot denote differentiation with respect to the material abscissa s and to time t, respectively. The second equation (2) is the compatibility equation, in which $\varepsilon = dS/ds - 1$ is the specific strain, with dS and ds the element lengths in $\mathcal{C}$ and $\overline{\mathcal{C}}$, respectively. The third and fourth equations (2) express the constitutive law; according to them, the tension $\mathbf{t}$ is directed along the tangent d$\mathbf{x}$/ds to the cable axis, and its modulus $T = \|\mathbf{t}\|$ grows with the axial rigidity EA proportionally to the strain ε, starting from the value $\bar{T}$ assumed in the reference configuration $\overline{\mathcal{C}}$.

Let $\mathbf{u} := \mathbf{x} - \overline{\mathbf{x}}$ the displacement measured from $\overline{\mathcal{C}}$ (Figure 1(c)); the equations (2), when projected on the base $\{\overline{\mathbf{a}}_i\}$, intrinsic to $\overline{\mathcal{C}}$, lead to:

$$\begin{aligned}
&\left[(\bar{T}+\hat{T})u_1'\right]' + \hat{b}_1 - m\ddot{u}_1 = 0\\
&\left[(\bar{T}+\hat{T})(u_2'+\kappa u_3)\right]' + \bar{\kappa}\hat{T} + \hat{b}_2 - m\ddot{u}_2 = 0\\
&\hat{T}' - (\bar{T}+\hat{T})\bar{\kappa}(u_2'+\bar{\kappa}u_3) + \hat{b}_3 - m\ddot{u}_3 = 0\\
&\frac{\hat{T}}{EA} = u_3' - \bar{\kappa}u_2 + \frac{1}{2}\left[u_1'^2 + (u_2'+\bar{\kappa}u_3)^2\right]
\end{aligned} \tag{3}$$

where $u_i := \mathbf{u}\cdot\overline{\mathbf{a}}_i$, $\hat{T} = EA\varepsilon$ is the increment of modulus of the tension, $\bar{\kappa}$ is the curvature in $\overline{\mathcal{C}}$; moreover, the strain is assumed small ($\varepsilon \ll 1$) and then the second equation (2) is expanded in series. The equations (3) have to be considered together with their boundary conditions $u_i(0) = 0$ ($i = 1, 2, 3$).

The cable profile can be assumed parabolic if the sag-span ratio is small (Irvine, 1981), $d/\ell \ll 1$, and the aerodynamic forces are uniform; furthermore, the approximations $\bar{\kappa} = 8d/\ell^2 = \text{constant}$ and $\bar{T} = \bar{b}\ell^2/8d = \text{constant}$ hold, with $\bar{b} = mg\cos\varphi - b_{a2}$ the resultant of self-weight and of aerodynamic force. Moreover, the tangential component of displacement u_3 can be statically condensed, thus giving (Lee and Perkins 1992):

$$\begin{aligned}
&(\bar{T}+EAe)u_1'' + \hat{b}_1 - m\ddot{u}_1 = 0\\
&(\bar{T}+EAe)u_2'' + \bar{\kappa}EAe + \hat{b}_2 - m\ddot{u}_2 = 0
\end{aligned} \tag{4}$$

where

$$e = -\frac{\bar{\kappa}}{\ell}\int_0^\ell u_2 \mathrm{d}s + \frac{1}{2\ell}\int_0^\ell \left(u_1'^2 + u_2'^2\right)\mathrm{d}s \tag{5}$$

is the specific strain, constant along the whole cable, $\varepsilon(s,t) \equiv e(t)$.

2.2. The aerodynamic model

The aerodynamic forces are deduced according to the quasi-steady theory (Blevins, 1990), neglecting the cable curvature and assuming that the iced cross-section is uniform. The twist angle of the section, induced by the transformation from $\mathcal{C}_0$ to $\overline{\mathcal{C}}$, is also taken into account and approximately set equal to φ (Figures 1 and 2), due to the smallness of the sag-to-span ratio; on the contrary, the rotation associated with the transformation from $\overline{\mathcal{C}}$ to $\mathcal{C}$ is neglected, since it cannot be described by a one-dimensional continuum of Cauchy (non-polar continuum) where the material points are not endowed with rotational degrees of freedom.

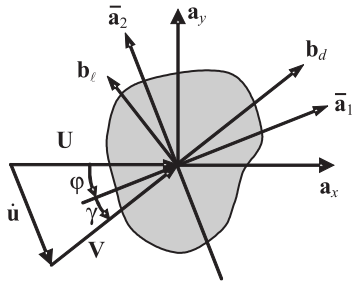

Figure 2. Wind action on the generic cross-section ($\mathbf{b}_d$ = drag force, $\mathbf{b}_\ell$ = lift force).

With reference to the generic cable cross-section (Figure 2), by assuming that the wind velocity $\mathbf{U} = U\mathbf{a}_x$ is orthogonal to the plane containing $\mathcal{C}_0$, the relative velocity $\mathbf{V} = \mathbf{U} - \dot{\mathbf{u}}$ forms an instantaneous angle of attack γ with the direction $\bar{\mathbf{a}}_1$, equal to

$$\gamma = \arcsin\left[\text{vers}\,\mathbf{V} \cdot \bar{\mathbf{a}}_2\right]. \tag{6}$$

The corresponding aerodynamic forces are expressed as (Figure 2)

$$\mathbf{b}_a = \frac{1}{2}\rho V r \left[c_d(\gamma)\mathbf{V} + c_\ell(\gamma)\mathbf{a}_3 \times \mathbf{V}\right] \tag{7}$$

with $c_d(\gamma)$ and $c_\ell(\gamma)$ the drag and lift coefficients, which depend on the angle of attack, ρ the air density, $V = \|\mathbf{V}\|$, and r a sectional characteristic dimension. By projecting the forces (7) on the base $(\bar{\mathbf{a}}_1, \bar{\mathbf{a}}_2)$ and expanding $\mathbf{V}$ and γ in MacLaurin series of the structural velocities $\dot{u}_1, \dot{u}_2$, the following components are obtained at the third order:

$$b_{ai} = \bar{b}_{ai} + \sum_{j=1}^{2} c_{ij}(\varphi)\dot{u}_j + \sum_{j,k=1}^{2} c_{ijk}(\varphi)\dot{u}_j\dot{u}_k + \sum_{j,k,l=1}^{2} c_{ijkl}(\varphi)\dot{u}_j\dot{u}_k\dot{u}_l \quad i = 1, 2. \tag{8}$$

The coefficients c_{ij}, c_{ijk}, c_{ijkl} depend on the angle φ, and are a combination of the aerodynamic coefficients c_d and c_ℓ and of their derivatives with respect to γ, all evaluated at $\gamma = -\varphi$, that is for $\dot{\mathbf{u}} \equiv \mathbf{0}$. A different level of approximation consists in considering the aerodynamic coefficients and their derivatives as calculated in $\gamma = 0$, and keeping their values constant for any value of U. This latter description of the cross-section aerodynamic properties is usually adopted in the galloping literature.

2.3. The non-dimensional equations of motion

The equations of motion (4) and (5), in non-dimensional form, read:

$$u_1'' - \Omega^2\ddot{u}_1 = \alpha u_1'' \left[\beta \int_0^1 u_2 \mathrm{d}s - \frac{1}{2}\int_0^1 (u_1'^2 + u_2'^2)\mathrm{d}s\right] - b_1(\dot{u}_1, \dot{u}_2)$$

$$u_2'' - \alpha\beta^2 \int_0^1 u_2 \mathrm{d}s - \Omega^2 \ddot{u}_2 = \alpha u_2'' \left[\beta \int_0^1 u_2 \mathrm{d}s - \frac{1}{2} \int_0^1 (u_1'^2 + u_2'^2) \mathrm{d}s \right]$$
$$- \frac{\alpha\beta}{2} \int_0^1 (u_1'^2 + u_2'^2) \mathrm{d}s - b_2(\dot{u}_1, \dot{u}_2) \quad (9)$$

with:

$$\tilde{u}_i = \frac{u_i}{\ell}; \quad \tilde{s} = \frac{s}{\ell}; \quad \tilde{t} = \omega t; \quad \Omega^2 = \frac{m\ell^2\omega^2}{\bar{T}}; \quad \tilde{b}_i = \frac{\hat{b}_i \ell}{\bar{T}};$$
$$\alpha = \frac{EA}{\bar{T}}; \quad \beta = \frac{8d}{\ell}; \quad \mu = \frac{\rho r U}{m\omega}; \quad \omega = \frac{\pi}{\ell}\sqrt{\frac{T_0}{m}} \quad (10)$$

where T_0 is the initial tension in $\mathcal{C}_0$ (i.e. in no-wind conditions), and the tilde has been omitted. Differently from previous approaches (Lee and Perkins, 1992; Luongo and Piccardo, 1998) a new definition of non-dimensional quantities has been adopted since a variable, fictitious, gravity force now acts on the inclined plane where the equilibrium is set. In equations (9) the incremental forces b_i assume expressions formally similar to (8), with the steady component deducted. However, in order to simplify their expression and according to results obtained in Luongo and Piccardo (1998), the quadratic terms are neglected leading to

$$b_i(\dot{u}_1, \dot{u}_2) = c_{i1}\dot{u}_1 + c_{i2}\dot{u}_2 + c_{i111}\dot{u}_1^3 + 3c_{i112}\dot{u}_1^2\dot{u}_2 + 3c_{i122}\dot{u}_1\dot{u}_2^2 + c_{i222}\dot{u}_2^3 \quad i = 1, 2. \quad (11)$$

The non-dimensional coefficients c_{ij} and c_{ijkl} are reported in the Appendix; they depend on the non-dimensional wind velocity μ, defined by the penultimate equation (10). The coefficients c_{11} and c_{22} also include viscous damping, assumed here as linear.

3. PERTURBATION ANALYSIS

The equations of motion (9) are solved through the Multiple Scale Method. It is well known that this method furnishes the bifurcation equations that rule the time evolution of amplitude and phase related to active modes (Luongo *et al*., 2003). When it is directly applied to partial derivative equations, it automatically takes into account the contribution of passive modes, which manifest themselves through the origin of "secondary modes", that are responsible for the spatial alteration of oscillation shapes, induced by the presence of nonlinearities (Rega *et al*., 1999).

The unknown displacements are developed in series of a perturbation parameter $\varepsilon \ll 1$:

$$u_i = \varepsilon u_{i1} + \varepsilon^2 u_{i2} + \varepsilon^3 u_{i3} + \ldots \quad i = 1, 2. \quad (12)$$

Then independent time scales are introduced $t_n = \varepsilon^n t (n = 0, 1, 2)$, so that the first and second time-derivatives are expressed as $\mathrm{D} = \mathrm{d}_0 + \varepsilon \mathrm{d}_1 + \varepsilon^2 \mathrm{d}_2 + \ldots$ and $\mathrm{D}^2 = \mathrm{d}_0^2 + 2\varepsilon \mathrm{d}_0\mathrm{d}_1 + \varepsilon^2(\mathrm{d}_1^2 + 2\mathrm{d}_0\mathrm{d}_2) + \ldots$, where $\mathrm{d}_n = \partial/\partial t_n$. Moreover, it is assumed that the linear dissipative

forces depending on velocities are small, that is $c_{ik} = \varepsilon \hat{c}_{ik}$, with $\hat{c}_{ik} = \mathrm{O}(1)$. Finally, the internal resonance condition between an in-plane mode (having a frequency equal to ω_2) and an out-of-plane mode (having a frequency equal to ω_1) is expressed through a detuning parameter $\sigma = \mathrm{O}(1)$:

$$\omega_2 = 2\omega_1 + \varepsilon\sigma\,. \tag{13}$$

The following perturbation equations are thus obtained.

Order ε:

$$u_{11}'' - \Omega^2 \mathrm{d}_0^2 u_{11} = 0 \tag{14a}$$

$$u_{21}'' - \alpha\beta^2 \int_0^1 u_{21}\mathrm{d}s - \Omega^2 \mathrm{d}_0^2 u_{21} = 0. \tag{14b}$$

Order ε^2:

$$u_{12}'' - \Omega^2 \mathrm{d}_0^2 u_{12} = 2\Omega^2 \mathrm{d}_0\mathrm{d}_1 u_{11} + \alpha\beta u_{11}'' \int_0^1 u_{21}\mathrm{d}s - c_{11}\mathrm{d}_0 u_{11} - c_{12}\mathrm{d}_0 u_{21} \tag{15a}$$

$$u_{22}'' - \alpha\beta^2 \int_0^1 u_{22}\mathrm{d}s - \Omega^2 \mathrm{d}_0^2 u_{22} = 2\Omega^2 \mathrm{d}_0\mathrm{d}_1 u_{21} + \alpha\beta u_{21}'' \int_0^1 u_{21}\mathrm{d}s$$

$$- \frac{\alpha\beta}{2} \int_0^1 \left({u_{11}'}^2 + {u_{21}'}^2\right) \mathrm{d}s - c_{21}\mathrm{d}_0 u_{11} - c_{22}\mathrm{d}_0 u_{21}. \tag{15b}$$

Order ε^3:

$$u_{13}'' - \Omega^2 \mathrm{d}_0^2 u_{13} = 2\Omega^2 \mathrm{d}_0\mathrm{d}_1 u_{12} + \Omega^2 \mathrm{d}_1^2 u_{11} + 2\Omega^2 \mathrm{d}_0\mathrm{d}_2 u_{11} + \alpha\beta u_{11}'' \int_0^1 u_{22}\mathrm{d}s$$

$$+ \alpha\beta u_{12}'' \int_0^1 u_{21}\mathrm{d}s - \frac{\alpha}{2} u_{11}'' \int_0^1 \left({u_{11}'}^2 + {u_{21}'}^2\right) \mathrm{d}s - c_{11}(\mathrm{d}_0 u_{12} + \mathrm{d}_1 u_{11})$$

$$- c_{12}(\mathrm{d}_0 u_{22} + \mathrm{d}_1 u_{21}) - c_{1111}(\mathrm{d}_0 u_{11})^3 - 3c_{1112}(\mathrm{d}_0 u_{11})^2 \mathrm{d}_0 u_{21}$$

$$- 3c_{1122}\mathrm{d}_0 u_{11}(\mathrm{d}_0 u_{21})^2 - c_{1222}(\mathrm{d}_0 u_{21})^3 \tag{16a}$$

$$u''_{23} - \alpha\beta^2 \int_0^1 u_{23}\mathrm{d}s - \Omega^2 \mathrm{d}_0^2 u_{23} = 2\Omega^2 \mathrm{d}_0\mathrm{d}_1 u_{22} + \Omega^2 \mathrm{d}_1^2 u_{21} + 2\Omega^2 \mathrm{d}_0\mathrm{d}_2 u_{21}$$

$$+ \quad \alpha\beta u''_{21} \int_0^1 u_{22}\mathrm{d}s + \alpha\beta u''_{22} \int_0^1 u_{21}\mathrm{d}s$$

$$- \quad \frac{\alpha}{2} u''_{21} \int_0^1 \left(u'^{\,2}_{11} + u'^{\,2}_{21}\right)\mathrm{d}s - \alpha\beta \int_0^1 \left(u'_{11}u'_{12} + u'_{21}u'_{22}\right)\mathrm{d}s$$

$$- \quad c_{21}(\mathrm{d}_0 u_{12} + \mathrm{d}_1 u_{11}) - c_{22}(\mathrm{d}_0 u_{22} + \mathrm{d}_1 u_{21}) - c_{2111}(\mathrm{d}_0 u_{11})^3 - 3c_{2112}(\mathrm{d}_0 u_{11})^2 \mathrm{d}_0 u_{21}$$

$$- \quad 3c_{2122}\mathrm{d}_0 u_{11}(\mathrm{d}_0 u_{21})^2 - c_{2222}(\mathrm{d}_0 u_{21})^3. \tag{16b}$$

The equations (14)–(16) have to be integrated with their boundary conditions

$$u_{ik}(0, t_n) = 0, \quad u_{ik}(1, t_n) = 0 \quad (i = 1, 2; \quad k = 1, 2, 3, \dots).$$

Equations (14) admit the following solution:

$$u_{k1} = A_k(t_1, t_2)\phi_k(s)\mathrm{e}^{\mathrm{i}\,\omega_k t_0} + \text{c.c.} \quad k = 1, 2 \tag{17}$$

where $\phi_k(s)$ are the eigenfunctions of the Hamiltonian system, corresponding to the two resonant frequencies; A_k are the complex amplitudes, which are unknowns functions of the slow times; the term c.c. denotes the complex conjugate. By substituting equations (17) into the right side of equations (15) and imposing the condition that it is orthogonal to solutions of the associated homogenous problem (solvability condition), we have:

$$\begin{aligned} \mathrm{d}_1 A_1 &= \frac{c_{11} A_1}{2\Omega^2} + \mathrm{i}\,\frac{\alpha\beta}{2\Omega^2\omega_1}\frac{I_1 I_{14}}{I_{11}}\bar{A}_1 A_2\,\mathrm{e}^{\mathrm{i}\,\sigma t_1} \\ \mathrm{d}_1 A_2 &= \frac{c_{22} A_2}{2\Omega^2} - \mathrm{i}\,\frac{\alpha\beta}{4\Omega^2\omega_2}\frac{I_1 I_3}{I_5}A_1^2\,\mathrm{e}^{-\mathrm{i}\,\sigma t_1} \end{aligned} \tag{18}$$

where I_i are integrals of the eigenfunctions $\phi_k(s)$ and their derivatives (see the Appendix). By substituting equations (18) into equations (15) and solving, one obtains:

$$\begin{aligned} u_{12} &= A_1 A_2 \psi_{12}\,\mathrm{e}^{\mathrm{i}(\omega_1+\omega_2)t_0} + \mathrm{i}\,A_2\psi_2\,\mathrm{e}^{\mathrm{i}\,\omega_2 t_0} + \text{c.c.} \\ u_{22} &= A_1^2\psi_{11}\,\mathrm{e}^{\mathrm{i}\,\omega_2 t_0}\,\mathrm{e}^{-\mathrm{i}\,\sigma t_1} + \mathrm{i}\,A_1\psi_1\,\mathrm{e}^{\mathrm{i}\,\omega_1 t_0} + A_2^2\psi_{22}\,\mathrm{e}^{2\,\mathrm{i}\,\omega_2 t_0} \\ &+ A_1\bar{A}_1\psi_{1\bar{1}} + A_2\bar{A}_2\psi_{2\bar{2}} + \text{c.c.} \end{aligned} \tag{19}$$

where the "secondary modes" $\psi_{ij}(s)$ are solution of the ordinary differential problems that are reported in the Appendix. They describe the alteration of the spatial shape of the re-

sponse, each of which is associated with a harmonic that takes part in the motion (base, sum and difference).

By substituting equations (18) and (19) into equations (16), and applying again the solvability condition, it is found that

$$\begin{aligned} \mathrm{d}_2 A_1 &= \mathrm{i}\, p_1 A_1 + \bar{A}_1 A_2 (p_{21} + \mathrm{i}\, p_{22})\, \mathrm{e}^{\mathrm{i}\sigma t_1} + A_1 A_2 \bar{A}_2 (p_{31} + \mathrm{i}\, p_{32}) \\ &+ A_1^2 \bar{A}_1 (p_{41} + \mathrm{i}\, p_{42}) \\ \mathrm{d}_2 A_2 &= \mathrm{i}\, p_5 A_2 + A_1^2 (p_{61} + \mathrm{i}\, p_{62})\, \mathrm{e}^{-\mathrm{i}\sigma t_1} + A_1 \bar{A}_1 A_2 (p_{71} + \mathrm{i}\, p_{72}) \\ &+ A_2^2 \bar{A}_2 (p_{81} + \mathrm{i}\, p_{82}) \end{aligned} \tag{20}$$

where the coefficients p are functions of the non-dimensional velocity μ and are defined in the Appendix. Finally, by combining equations (18) and (20) according to the reconstitution rule $\dot{A}_k = \varepsilon \mathrm{d}_1 A_k + \varepsilon^2 \mathrm{d}_2 A_k$, and then reabsorbing the perturbation parameter in the coefficients, one obtains the (complex) bifurcation equations, which are of the type $\dot{A}_k = f_k(A_1, A_2)$ $(k = 1, 2)$. They can be written in real form adopting the polar representation $A_k = 1/2\, a_k\, \mathrm{e}^{\mathrm{i}\theta_k}$, with a_k the real amplitude and θ_k the phase. Finally, by defining the phase difference

$$\delta := \theta_2 - 2\theta_1 + \sigma t \tag{21}$$

the (real) bifurcation equations are reduced to three equations, having an autonomous form:

$$\begin{cases} \dot{a}_1 = a_1 \left[\dfrac{c_{11}}{2\Omega^2} + \dfrac{1}{2} a_2 (p_{21} \cos\delta - p_{22}^* \sin\delta) + \dfrac{1}{4} a_2^2 p_{31} + \dfrac{1}{4} a_1^2 p_{41} \right] \\ \dot{a}_2 = a_2 \dfrac{c_{22}}{2\Omega^2} + \dfrac{1}{2} a_1^2 (p_{61} \cos\delta + p_{62}^* \sin\delta) + \dfrac{1}{4} a_1^2 a_2 p_{71} + \dfrac{1}{4} a_2^3 p_{81} \\ a_1 a_2 \dot{\delta} = a_1 \left[a_2 (p_5 - 2p_1 + \sigma) - a_2^2 (p_{21} \sin\delta + p_{22}^* \cos\delta) \right. \\ \qquad + \dfrac{1}{2} a_1^2 (-p_{61} \sin\delta + p_{62}^* \cos\delta) + \dfrac{1}{4} a_2^3 (p_{82} - 2p_{32}) \\ \qquad \left. + \dfrac{1}{4} a_1^2 a_2 (p_{72} - 2p_{42}) \right] \end{cases} \tag{22}$$

where two new coefficients appear, also defined in the Appendix. Equations (22) are formally identical to those already found in Luongo and Piccardo (1998), but the expression for coefficients p is very different because of the presence of the secondary modes ψ, which were previously absent.

4. AMPLITUDE EQUATION ANALYSIS

The fixed points (a_1, a_2, δ) of the dynamical system (22) correspond to steady-state solutions of the original system (9). By truncating the expansion (12) at the ε^2-order, steady-state solutions of equations (22) are found to be

$$\begin{aligned} u_1(s,t) &= a_1\phi_1(s)\cos\Omega_1 t + \frac{1}{2}a_1a_2\psi_{12}(s)\cos(3\Omega_1 t+\delta) - a_2\psi_2(s)\sin(\Omega_2 t+\delta) \\ u_2(s,t) &= a_2\phi_2(s)\cos(\Omega_2 t+\delta) + \frac{1}{2}a_1^2\psi_{11}(s)\cos\Omega_2 t - a_1\psi_1(s)\sin\Omega_1 t \\ &+ \frac{1}{2}a_2^2\psi_{22}(s)\cos[2(\Omega_2 t+\delta)] + \frac{1}{2}a_1^2\psi_{1\bar{1}}(s) + \frac{1}{2}a_2^2\psi_{2\bar{2}}(s) \end{aligned} \tag{23}$$

where an arbitrary initial phase has been set equal to zero. In equations (23)

$$\begin{aligned} \Omega_1 &= \omega_1 + p_1 + \frac{1}{2}a_2\left(p_{21}\sin\delta + p_{22}^*\cos\delta\right) + \frac{1}{4}a_2^2p_{32} + \frac{1}{4}a_1^2p_{42} \\ \Omega_2 &= \omega_2 + p_5 + \frac{1}{2}\frac{a_1^2}{a_2}\left(-p_{61}\sin\delta + p_{62}^*\cos\delta\right) + \frac{1}{4}a_1^2p_{72} + \frac{1}{4}a_2^2p_{82} \end{aligned} \tag{24}$$

are the amplitude-dependent frequencies of the periodic motion (non-linear frequencies). In equations (24) the terms p_1 and p_5 represent the correction of the linear undamped frequencies due to the damping terms c_{ij} $(i, j = 1, 2)$. At the leading order the in-plane displacement u_2 oscillates at a frequency double that of the out-of-plane displacement u_1, with a phase-difference δ.

From the analysis of equations (22) the existence of the following branches of fixed points is proved (Luongo and Piccardo 1998): *branch I*, $a_1 = a_2 = 0$, δ arbitrary, $\forall\ \mu$; *branch II*, $a_1 = 0$, $a_2 = a_2(\mu) = \sqrt{-2c_{22}/(\Omega^2 p_{81})}$, δ arbitrary; *branch III*, $a_1 = a_1(\mu)$, $a_2 = a_2(\mu)$, $\delta = \delta(\mu)$.

The bifurcation of branch I occurs when $a_1 \to 0$, $a_2 \to 0$, $\mu \to \mu_{cr}$; then, the equations (22) reduce to

$$a_1\frac{c_{11}^{cr}}{2\Omega^2} = 0, \quad a_2\frac{c_{22}^{cr}}{2\Omega^2} = 0, \quad a_1a_2\left(p_5^{cr} - 2p_1^{cr} + \sigma\right) = 0 \tag{25}$$

where the apex cr means that quantities are evaluated at $\mu = \mu_{cr}$. Two different solutions of equations (25) exist: a_2-bifurcation, $a_1 = 0$, $a_2 \neq 0$ when $c_{22}^{cr} = 0$; a_1-bifurcation, $a_1 \neq 0$, $a_2 = 0$ when $c_{11}^{cr} = 0$. In the first case the branch bifurcates in a_2-direction, while, in the second case, it bifurcates in a_1-direction. However, if the static rotation of cable is null $(\varphi = 0)$, the coefficient c_{11} is always negative for any value of μ, due to the physics of the problem (the drag coefficient c_d is positive for any kind of cross-section); therefore, critical conditions in a_1-direction can occur for high value of rotation φ only (i.e. very large mean wind speed). In both cases galloping is mono-modal, since only one mode is triggered at bifurcation. In the sequel of the paper the name "branch II" denotes a bifurcation in a_2-direction.

Finally, the bifurcation of branch II is analyzed. To this end one looks for the existence of two-component solutions ($a_1 \neq 0$, $a_2 \neq 0$) close to the branch $(a_1, a_2) = (0, a_2(\mu))$. By resolving the limit of equations (22) for $a_1 \to 0$, $\delta \to \delta_0$, $\mu \to \mu_0$, $a_2 \to a_{20}$, with $a_{20} = a_2(\mu_0)$, the following equations are obtained:

$$\begin{cases} \dfrac{c_{11}^0}{2\Omega^2} + \dfrac{1}{2}a_{20}(p_{21}^0 \cos\delta_0 - p_{22}^{*0} \sin\delta_0) + \dfrac{1}{4}a_{20}^2 p_{31}^0 = 0 \\ a_{20}(p_5^0 - 2p_1^0 + \sigma) - a_{20}^2(p_{21}^0 \sin\delta_0 + p_{22}^{*0} \cos\delta_0) + \dfrac{1}{4}a_{20}^3(p_{82}^0 - 2p_{32}^0) = 0 \end{cases} \tag{26}$$

where the apex 0 means that coefficients c and p are evaluated at $\mu = \mu_0$; the second part of equation (22) doesn't appear, since it reduces to an identity at the leading order. Equations (26) are a non-linear algebraic system in the two unknowns, δ_0 and μ_0. Each solution of this system determines a bifurcation point on the branch II, from which a branch III originates. Bi-modal galloping occurs along this path as a consequence of the non-linear interaction between the two internally resonant modes, mainly governed by quadratic mechanical terms.

Concerning the role of secondary modes on the fixed point branches, it should be noted that they appear only in the bifurcation of branch II through some of the coefficients p in the second part of equation (26). Therefore, their influence on system stability is limited to bi-modal galloping cases; their effective importance can be verified on numerical examples. On the other hand, the secondary modes can notably modify the shape of steady-state solutions through the spatial functions $\psi(s)$, as clearly highlighted by equations (23).

5. NUMERICAL RESULTS

In order to numerically verify the analytical procedure, a real iced cable, already investigated in the literature through a discrete solution (Luongo and Piccardo, 1998), has been taken into account. This basic example concerns a U-shaped conductor with a symmetric section having its maximum ice eccentricity opposite to the mean wind; the idealized aerodynamic coefficients are: $c_d(\gamma) = 1.0833 + 0.73594\gamma^2$, $c_l(\gamma) = -1.5979\gamma + 4.77362\gamma^3$, that are assumed valid in the range $-0.6 < \gamma < 0.6$. This cross-section is more prone to galloping when the angle of attack γ is zero. The cable has a diameter of 2.81 cm, a mass of 1.80 kg/m (ice included), damping coefficients equal to 0.44% and axial rigidity of 29.7×10^6 N.

First, following the literature approach, the aerodynamic coefficients are evaluated in the initial configuration of equilibrium $\mathcal{C}_0$, that is for $\gamma = 0$, and are maintained constant when the mean wind velocity is varying. The implications of this hypothesis will be considered further on. In no-wind conditions the cable is characterized by the non-dimensional coefficients $\alpha = 1165$ and $\beta = 0.185$; therefore, according to the Irvine parameter $\lambda^2 = \alpha\beta^2 \simeq 4\pi^2$, the cable is close to the first cross-over point ($\omega_1 = 1$, $\omega_2 = 2.00663$). When the non-dimensional mean wind velocity μ is varying, the equilibrium path $\varphi = \varphi(\mu)$ is deduced (Figure 3(a)). As a consequence, the cable mechanical parameters are modified; Figure 3(b) and 3(c) show the changes in the reference tension $\bar{T}$ and in the cable parameter α, respectively.

By solving the eigenvalue problem of the linearized equations of cable, one obtains the behaviour of the frequencies of active modes (Figure 4(a)); when μ assumes values

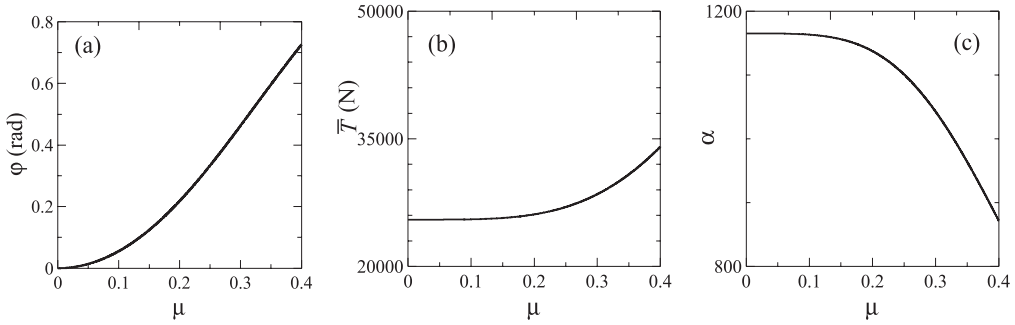

Figure 3. (a) Static rotation of the cable; (b) reference tension; (c) cable parameter α.

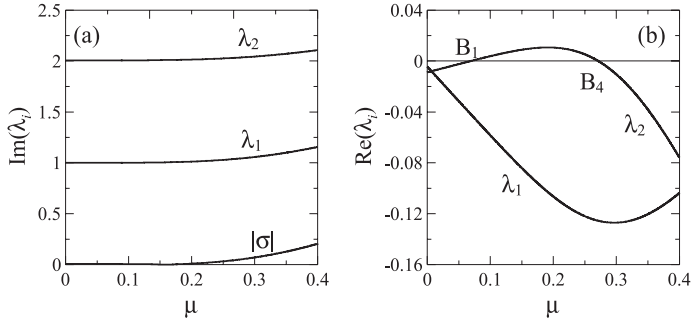

Figure 4. Eigenvalues of the linearized equations: (a) imaginary part; (b) real part.

greater than 0.3, the cable begins to sensibly move away from the initial condition of internal resonance 1 : 2. The real part of the eigenvalues (Figure 4(b)) has been deduced from the linear terms of the amplitude equations (22); it is characterized by a first point of bifurcation B_1, at a relatively low wind velocity, and a re-entry bifurcation point B_4, both on the in-plane eigenvalue λ_2. In particular, the point B_4 doesn't appear in the classic galloping problems deduced from sectional models (Blevins, 1990) and it is clearly due to the modification induced by the static rotation φ. By surveying the expressions for non-dimensional linear aerodynamic coefficients c_{ij} (reported in the Appendix) it is evident that their values can be altered by the presence of angle φ. Even if the cross-section is initially symmetrical, as in the present example, the linear aerodynamic damping matrix is always full for any value of μ (i.e. φ) different from zero.

From the observation that cable parameters vary with μ, it follows that a family of cables is considered, exploring a range of mean wind velocities. Therefore, both the primary modes $\phi_i(s)$ and the secondary modes $\psi(s)$ of the cable undergo changes when μ is growing (Figure 5). In particular, the tangent at the boundaries of the in-plane mode $\phi_2(s)$ rotates (becoming similar to taut string modes), whereas the out-of-plane mode is unchanged (Figure 5(a)). Secondary modes (Figure 5(b)–(h)) are evaluated in two different ways, exactly (i.e. by solving the o.d.e. reported in the Appendix) or by a Galerkin procedure. In this latter case it

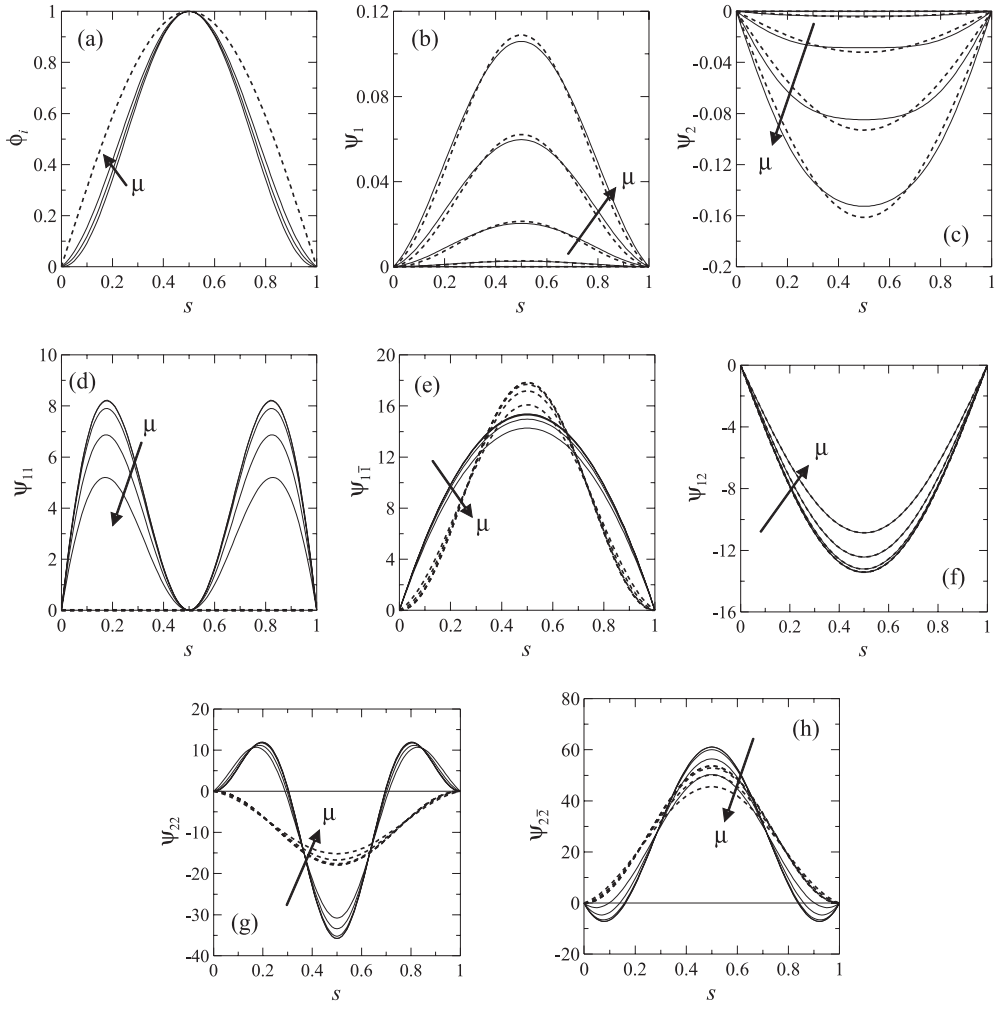

Figure 5. (a) Cable primary modes $\phi_i(s)$ (ϕ_1: dashed lines; ϕ_2: thin lines); (b)–(h) cable secondary modes (complete solutions: thin lines; Galerkin approximations (27): dashed lines). Arrows indicate the growing direction of μ ($\mu = 0$, 0.1, 0.2, 0.3, 0.4).

is possible to neglect the contribution of passive modes and, therefore, to have a solution comparable to the discrete approaches in the literature (Luongo and Piccardo 1998). Since the generic differential equation in $\psi(s)$ is of the type $\mathrm{L}\psi(s) - b(s) = 0$, with $\mathrm{L} := \mathrm{D} + \Omega^2\hat{\omega}^2$, the one-mode Galerkin approximation furnishes

$$\psi(s) = \frac{1}{\Omega^2\left(\hat{\omega}^2 - \omega_j^2\right)} \frac{\int_0^1 b(s)\phi_j(s)\mathrm{d}s}{\int_0^1 \phi_j^2(s)\mathrm{d}s}\phi_j(s) \tag{27}$$

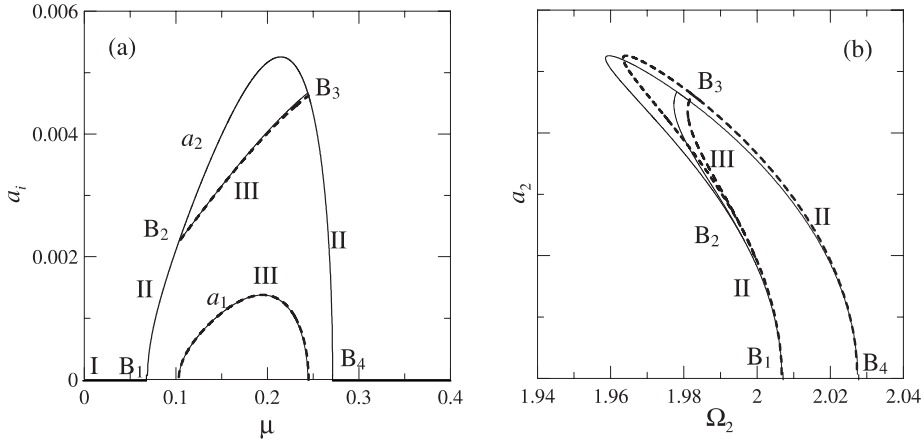

Figure 6. (a) Active modal amplitudes and (b) non-linear in-plane frequency; complete solution (thin lines) and active mode solution (dashed lines).

where $j = 1, 2$ according to whether ψ is related to the first or second primary mode of the cable. Figure 5(b)–(h) highlights that in some cases the Galerkin approximation is good or very good (ψ_1, ψ_2, ψ_{12}), whereas in others it leads to rough approximations. This fact implies that, at least potentially, passive modes could influence the response of such a system. To verify the extent of such an occurrence the analysis of nonlinear post-critical paths is necessary.

Figure 6 shows a comparison between the continuous system, with a correct evaluation of passive modes, and an equivalent discrete system, where the secondary modes are approximated by equation (27). The post-critical branches present all the cases outlined in the previous section. Concerning the non-linear in-plane frequency (Figure 6(b)), it originates from the linear damped frequency, close to $\omega_2 = 2$, it has a softening behaviour until a_2 reaches a maximum, then it has a hardening behaviour until a_2 vanishes. It should be noted that this example is marginally influenced by passive modes, both for the motion amplitudes and for the non-linear frequencies. An explanation of this result can be found by analyzing in more detail equations (26) governing the bifurcation points B_2 and B_3 (between branches II and III). In them, the sole terms influenced by secondary modes are the linear and the cubic terms in the second part of (26). But the linear term depends on p_1 and p_5 coefficients, which in turn depend on Ψ_1 and Ψ_2, which are well approximated by the Galerkin procedure. Therefore, one needs to have a sufficiently high value of in-plane amplitude a_2 to obtain a significant contribution by secondary modes. On the other hand, the branch II has a characteristic "bell" shape due to the alteration induced by the static rotation φ, which causes a decreasing of aerodynamic forces starting from the worst conditions (i.e. from the value of coefficients more prone to galloping). Thus, it's not so easy to reach high value of in-plane amplitude for this system typology. Comparison of the steady-state time-histories and trajectories (Figure 7, obtained for $\mu = 0.194$, close to the maximum value of out-of-plane amplitude a_1) confirms the previous observations. In the middle point of the cable ($s = 0.5$) there is a slight difference in the maximum values and in the frequency of the in-plane mo-

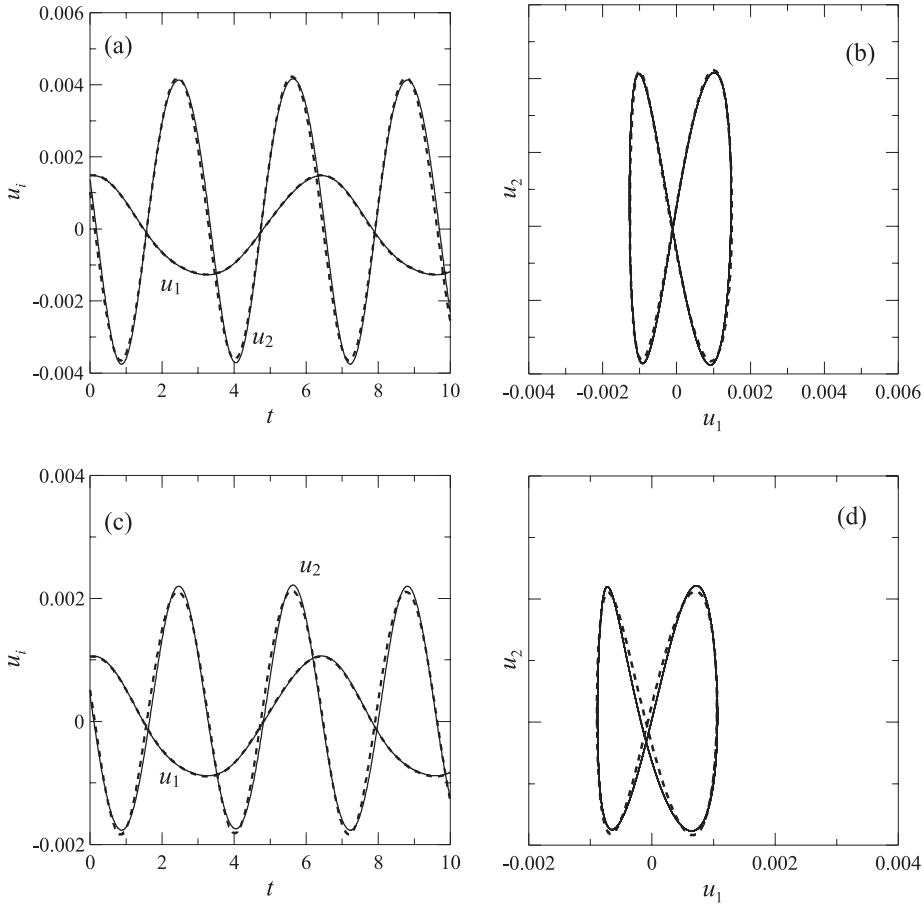

Figure 7. Steady-state motions and trajectories ($\mu = 0.194$): (a), (b) $s = 0.5$; (c), (d) $s = 0.25$; complete solution (thin lines) and active mode solution (dashed lines).

tion. A little more relevant variations appear at the quarter point ($s = 0.25$) concerning the maximum amplitude of the in-plane oscillations.

In order to verify this kind of behaviour on other examples, a non-symmetric cross-section in no-wind conditions is considered, again taken from previous papers (Luongo and Piccardo 1998). The cross-section is still a U-shaped conductor, but now stressed by a rotated flow of about 44° with respect to the symmetry axis. As regards the basic example this new iced section has thus different aerodynamic coefficients and mass (2.00 kg/m ice included) since it has a greater ice thickness. The post-critical branches and the non-linear frequencies are depicted in Figure 8. As regards the foregoing example no substantial difference appears. The complete in-plane amplitude and non-linear frequency are slightly more distinct from the approximate ones, but this fact is attributable to the greater level of oscillations that this cross-section permits (and not on the different type of section geometry in no-wind conditions). An attempt to amplify differences between the two levels of solution has been taken into account, modifying the aerodynamic characteristics of the cross-section (the value

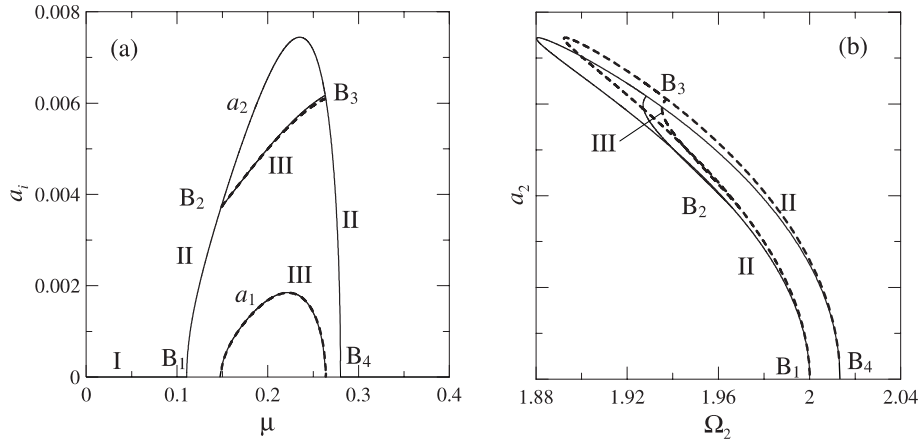

Figure 8. (a) Active modal amplitudes and (b) non-linear in-plane frequency for a cross-section non-symmetric in no-wind conditions; complete solution (thin lines) and active mode solution (dashed lines). Aerodynamic cross-section coefficients are: $c_d = 1.1847$, $c_l = 0.29813$, $c'_d = 1.3319$, $c'_l = -1.3736$, $c''_d = -0.62865$, $c''_l = -0.0076683$, $c'''_d = -27.790$, $c'''_l = 34.374$.

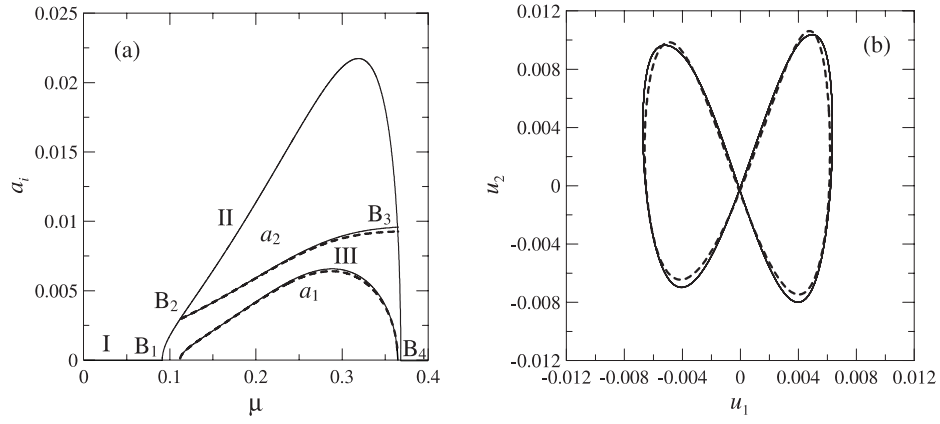

Figure 9. (a) Active modal amplitudes and (b) steady-state trajectories ($\mu = 0.29$, $s = 0.5$) for a modified non symmetric cross-section; complete solution (thin lines) and active mode solution (dashed lines).

of the first derivate of the drag coefficient, c'_d, has been increased to 3). In this way the amplitudes of active modes are notably increased obtaining a more remarkable difference between the complete solution and the approximate one (Figure 9). In any case the branch III (Figure 9(a)) is rather self-limiting and doesn't permit to obtain still larger alterations. The steady-state trajectories (Figure 9(b)) highlight an appreciable modification of the in-plane motion.

Finally, concerning the aerodynamic description of the cross-section (Section 2.2) two different levels of approximation can be assumed (Figure 10(a)). The first approach, adopted until now, considers the aerodynamic coefficients calculated in the initial configuration $\mathcal{C}_0$

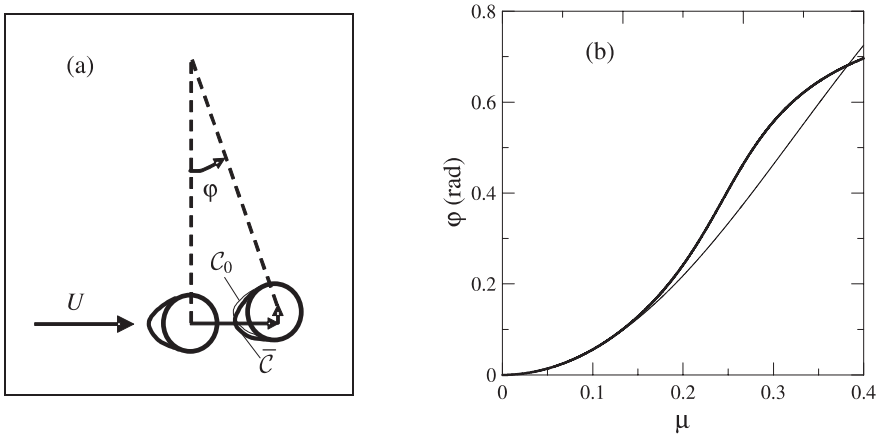

Figure 10. (a) Aerodynamic coefficients calculated in initial or reference configuration; (b) static rotation of the cable (initial configuration $\mathcal{C}_0$: thin lines; reference configuration $\overline{\mathcal{C}}$: thick lines). Aerodynamic coefficients are related to the basic example.

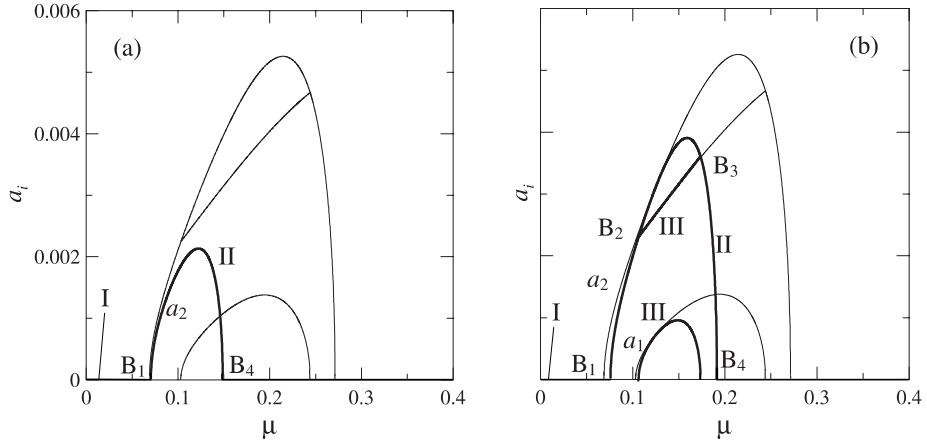

Figure 11. Active modal amplitudes with aerodynamic coefficients in initial (thin lines) or reference (thick lines) configuration, where γ is initially assumed equal to (a) 0° or (b) 5°. Aerodynamic coefficients are related to the basic example.

($\gamma = 0$), without any modification of their value during the computation. The second approach, surely more precise but not present in the literature to the author's knowledge, computes the aerodynamic coefficients in the reference configuration $\overline{\mathcal{C}}$, that is for the angle of attack equal to the static rotation, unless the sign ($\gamma = -\varphi$). A first comparison between the two different approaches concerns the evaluation of the equilibrium path $\varphi = \varphi(\mu)$, shown in Figure 10(b) for the basic cross-section; the alterations are remarkable, even for limited values of mean wind velocity. This fact can involve very important changes in the post-critical branches. Figure 11(a) shows the active modal amplitudes related to the two different levels

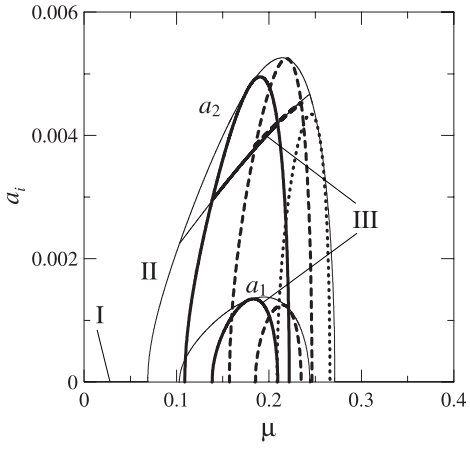

Figure 12. Active modal amplitudes with aerodynamic coefficients in initial (thin lines) or reference configuration, with γ initially assumed equal to 10° (thick lines), 15° (dashed lines) and 20° (dot lines). Aerodynamic coefficients are related to the basic example.

of approximation, starting from the cross-section aerodynamic parameters more prone to galloping in no-wind conditions. The first bifurcation point remains unchanged but the re-entry point is notably influenced by the alteration of the value of aerodynamic coefficients due to the static rotation. As a consequence the post-critical branches are greatly modified. The aerodynamic coefficients move away from the more dangerous values when μ is increasing, thus the branch III is completely destroyed. If the analysis starts with the same cross-section rotated in an initial position suitably distinct from the more prone to galloping (e.g. 5° away, Figure 11(b)), the cable arrives at the more dangerous configuration just in the proximity of the first bifurcation point B_1. In this way branches reach a larger development, with the return of branch III, but the post-critical behaviour is significantly different from that obtained with unchanged aerodynamic properties. Starting the analysis with cross-sections ever more initially rotated (i.e. $\gamma = 10°, 15°, 20°$), the instability may be found at higher critical velocities but the phenomenon is not simply translated in the wind-speed range (Figure 12). Actually, all the cases examined are completely enveloped by the basic example obtained with constant aerodynamic coefficients. This fact confirms that, for the same aerodynamic characteristics, the re-entry bifurcation is mainly governed by the mean flow, which implies an inclined equilibrium position (Figure 10(a)). Moreover, the nonlinear behaviours are very diversified when the initial position of the section is varying, with the possibility of achieving a bi-modal galloping only if the in-plane amplitude a_2 reaches sufficiently high values.

6. CONCLUSIONS AND PERSPECTIVES

This paper is concerned with the analysis of the aeroelastic behaviour of cables with small sag-to-span ratio, in internal resonance conditions, subjected to a uniform wind. The Multiple Scale Method has been applied to the partial derivative non-linear equations of motion,

avoiding recourse to any discretization techniques. The following conclusions can be drawn. (1) The proposed analytical procedure appears more straightforward than for previous discrete solutions (e.g. Luongo and Piccardo, 1998), being able to highlight the contribution of static rotation and to take into account the secondary (passive) modes of the cable. (2) The passive modes seems to have a small influence on the bifurcation curves, at least for the values of in-plane amplitude achieved here (only the branch III is slightly modified); their importance grows as regards the steady-state deflection shapes and trajectories. (3) The static rotation of the cable has, on the contrary, remarkable effects on the system dynamics via the modification of both the coefficients of aerodynamic forces (c_{ij}, c_{ijk}, c_{ijkl}), and the drag and lift aerodynamic coefficients (c_d, c_l). (4) Due to the static rotation, galloping in cables appears as a bound phenomenon, valid only for a suitable range of mean wind velocities. This result is very different from the usual galloping diagram where the phenomenon starts at a critical velocity and continues indefinitely for any velocity greater than the critical one. (5) Taking into account correctly the variation of aerodynamic coefficients (drag and lift) with the static rotation, the possibility to have a bi-modal galloping (branch III) is due to the initial rotation of the cross-section. In the usual galloping analysis, the aerodynamic coefficients more prone to galloping are those in no-wind conditions; here, the attainment of this value of coefficients for a suitable static rotation (different from zero) can be more dangerous. The usual case of constant aerodynamic coefficients seems to be a protective approach, at least in the limits of the present analysis, since it envelops any possible situation of variable aerodynamic coefficients.

To sum up, the present approach with two sole active symmetric modes represents a first step in the full comprehension of the nonlinear multi-mode galloping of suspended cables. It is expected that also resonant skew-symmetric modes may be involved in the system dynamics (Rega *et al*., 1999), making it necessary to consider a greater number of active modes. But, before continuing in this direction, a detailed investigation is required of the scenario of all the critical conditions, that could occur also on skew-symmetric modes, as confirmed by preliminary investigations. Moreover, a further refinement of the mechanical model employed here concerns the possibility of considering the torsional rotation of the cable in the dynamic field, formulating a model of curved elastic prestressed beam subjected to aerodynamic forces (Luongo *et al*., 2006).

APPENDIX

Non-dimensional aerodynamic coefficients

$$
\begin{aligned}
c_{11} &= -\frac{1}{2}\mu\Omega^2\left[c_d(1+\cos^2\varphi)+(c_\ell+c'_d)\sin\varphi\cos\varphi+c'_\ell\sin^2\varphi\right]-2\xi_1\omega_1\Omega^2\\
c_{12} &= \frac{1}{2}\mu\Omega^2\left[c_\ell(1+\sin^2\varphi)+(c_d-c'_\ell)\sin\varphi\cos\varphi-c'_d\cos^2\varphi\right]\\
c_{21} &= \frac{1}{2}\mu\Omega^2\left[-c_\ell(1+\cos^2\varphi)+(c_d-c'_\ell)\sin\varphi\cos\varphi+c'_d\sin^2\varphi\right]
\end{aligned}
$$

$$
\begin{aligned}
c_{22} &= \frac{1}{2}\mu\Omega^2\left[-c_d(1+\sin^2\varphi)+(c'_d+c_\ell)\sin\varphi\cos\varphi-c'_\ell\cos^2\varphi\right]-2\xi_2\omega_2\Omega^2\\
c_{1111} &= -\frac{1}{12}\frac{k^2\Omega^2}{\mu}c_{a1}\sin^3\varphi;\quad c_{1112}=-\frac{1}{12}\frac{k^2\Omega^2}{\mu}c_{a1}\sin^2\varphi\cos\varphi;\\
c_{1122} &= -\frac{1}{12}\frac{k^2\Omega^2}{\mu}c_{a1}\sin\varphi\cos^2\varphi;\quad c_{1222}=-\frac{1}{12}\frac{k^2\Omega^2}{\mu}c_{a1}\cos^3\varphi;\\
c_{2111} &= -\frac{1}{12}\frac{k^2\Omega^2}{\mu}c_{a2}\sin^3\varphi;\quad c_{2112}=-\frac{1}{12}\frac{k^2\Omega^2}{\mu}c_{a2}\sin^2\varphi\cos\varphi;\\
c_{2122} &= -\frac{1}{12}\frac{k^2\Omega^2}{\mu}c_{a2}\sin\varphi\cos^2\varphi;\quad c_{2222}=-\frac{1}{12}\frac{k^2\Omega^2}{\mu}c_{a2}\cos^3\varphi
\end{aligned}
$$

with

$$
\begin{aligned}
k &= \frac{\rho r\ell}{m};\quad c_{a1}=\left[c'_d-3(c_\ell+c''_\ell)+c'''_d\right]\cos\varphi+\left[c'_\ell+3(c_d+c''_d)+c'''_\ell\right]\sin\varphi\\
c_{a2} &= -\left[c'_d-3(c_\ell+c''_\ell)+c'''_d\right]\sin\varphi+\left[c'_\ell+3(c_d+c''_d)+c'''_\ell\right]\cos\varphi.
\end{aligned}
$$

Integrals of eigenfunctions of the cable active modes

$$
\begin{aligned}
I_1 &= \int_0^1\phi_2\mathrm{d}s;\quad I_2=\int_0^1\phi_2'^2\mathrm{d}s;\quad I_3=\int_0^1\phi_1'^2\mathrm{d}s;\quad I_5=\int_0^1\phi_2^2\mathrm{d}s;\\
I_9 &= \int_0^1\phi_2^4\mathrm{d}s;\quad I_{11}=\int_0^1\phi_1^2\mathrm{d}s;\quad I_{14}=\int_0^1\phi_1\phi_1''\mathrm{d}s;\quad I_{16}=\int_0^1\phi_1^4\mathrm{d}s;\\
I_{17} &= \int_0^1\phi_1^2\phi_2^2\mathrm{d}s;\quad I_{18}=\int_0^1\phi_2\phi_2''\mathrm{d}s.
\end{aligned}
$$

Differential problems of cable secondary modes

$$
\begin{aligned}
&\psi''_{12}+\Omega^2(3\omega_1)^2\psi_{12}=\alpha\beta\phi''_1I_1;\quad \psi''_2+\Omega^2\omega_2^2\psi_2=-c_{12}\omega_2\phi_2;\\
&\psi''_{11}-\alpha\beta^2\int_0^1\psi_{11}\mathrm{d}s+\Omega^2\omega_2^2\psi_{11}=\frac{\alpha\beta}{2}\left(\frac{I_1I_3}{I_5}\phi_2-I_3\right);\\
&\psi''_1-\alpha\beta^2\int_0^1\psi_1\mathrm{d}s+\pi^2\psi_1=-c_{21}\omega_1\phi_1;
\end{aligned}
$$

$$\psi''_{22} - \alpha\beta^2 \int_0^1 \psi_{22} \mathrm{d}s + \Omega^2 (2\omega_2)^2 \psi_{22} \;=\; \alpha\beta \left(\phi''_2 I_1 - \frac{I_2}{2} \right);$$

$$\psi''_{1\bar{1}} - \alpha\beta^2 \int_0^1 \psi_{1\bar{1}} \mathrm{d}s \;=\; -\frac{\alpha\beta}{2} I_3; \quad \psi''_{2\bar{2}} - \alpha\beta^2 \int_0^1 \psi_{2\bar{2}} \mathrm{d}s \;=\; \alpha\beta \left(-\frac{I_2}{2} + \phi''_2 I_1 \right).$$

Coefficients of the bifurcation equations

$$\begin{aligned}
p_1 &= \frac{1}{2\Omega^2\omega_1} \left(c_{12}\omega_1 \frac{J_7}{I_{11}} - \frac{c_{11}^2}{4\Omega^2} \right); \quad p_{21} = -\frac{1}{2\Omega^2\omega_1 I_{11}} \left(\frac{\alpha\beta c_{22}}{4\Omega^2\omega_1} I_1 I_{14} \right); \\
p_{22} &= -\frac{1}{2\Omega^2\omega_1 I_{11}} \left(\frac{\alpha\beta}{2\omega_1} I_1 I_{14} \sigma \right); \quad p_{31} = \frac{3c_{1122}\omega_2^2 I_{17}}{\Omega^2 I_{11}}; \\
p_{32} &= -\frac{1}{2\Omega^2\omega_1 I_{11}} \left[-\frac{(\alpha\beta I_1 I_{14})^2}{4\omega_1^2\Omega^2 I_{11}} + \alpha I_2 I_{15} - 2\alpha\beta I_{14} J_4 - \alpha\beta I_1 J_6 \right]; \\
p_{41} &= \frac{3c_{1111}\omega_1^2 I_{16}}{2\Omega^2 I_{11}}; \\
p_{42} &= -\frac{1}{2\Omega^2\omega_1 I_{11}} \left(\frac{3}{2}\alpha I_3 I_{14} - \alpha\beta I_{14} J_2 - 2\alpha\beta I_{14} J_3 - \frac{\alpha^2\beta^2 I_1^2 I_3 I_{14}}{8\Omega^2\omega_1\omega_2 I_5} \right) \\
p_5 &= \frac{1}{2\Omega^2\omega_2} \left(\frac{c_{21}\omega_2 J_{18}}{I_5} - \frac{c_{22}^2}{4\Omega^2} \right); \\
p_{61} &= -\frac{1}{2\Omega^2\omega_2 I_5} \left(2c_{11}\omega_2 J_8 - c_{22}\omega_2 J_8 - \frac{\alpha\beta c_{11} I_1 I_3}{4\Omega^2\omega_2} + \frac{\alpha\beta c_{22} I_1 I_3}{8\Omega^2\omega_2} \right); \\
p_{62} &= -\frac{1}{2\Omega^2\omega_2 I_5} \left(-2\Omega^2\omega_2 J_8 \sigma + \frac{\alpha\beta I_1 I_3 \sigma}{4\omega_2} \right); \quad p_{71} = \frac{3c_{2112}\omega_1^2 I_{17}}{\Omega^2 I_5}; \\
p_{72} &= -\frac{1}{2\Omega^2\omega_2 I_5} \left(\frac{2\alpha\beta\omega_2 I_1 I_{14} J_8}{\omega_1 I_{11}} - \frac{\alpha^2\beta^2 I_1^2 I_3 I_{14}}{4\Omega^2\omega_1\omega_2 I_{11}} + \alpha I_3 I_{18} - 2\alpha\beta I_1 J_{11} \right. \\
&+ \left. \alpha\beta I_1 J_{14} + 2\alpha\beta I_1 J_{16} - 2\alpha\beta I_{18} J_3 \right); \quad p_{81} \;=\; \frac{3c_{2222}\omega_2^2 I_9}{2\Omega^2 I_5} \\
p_{82} &= \frac{1}{2\Omega^2\omega_2 I_5} \left(-\frac{3}{2}\alpha I_2 I_{18} + \alpha\beta I_1 J_{10} + 2\alpha\beta I_1 J_{12} - \alpha\beta I_1 J_{15} \right. \\
&- \left. 2\alpha\beta I_1 J_{17} + 2\alpha\beta I_{18} J_4 + \alpha\beta I_{18} J_9 \right)
\end{aligned}$$

with

$$J_2 = \int_0^1 \psi_{11}\mathrm{d}s; \quad J_3 = \int_0^1 \psi_{1\bar{1}}\mathrm{d}s; \quad J_4 = \int_0^1 \psi_{2\bar{2}}\mathrm{d}s; \quad J_6 = \int_0^1 \phi_1\psi''_{12}\mathrm{d}s;$$

$$J_7 = \int_0^1 \phi_1\psi_1\mathrm{d}s; \quad J_8 = \int_0^1 \phi_2\psi_{11}\mathrm{d}s; \quad J_9 = \int_0^1 \psi_{22}\mathrm{d}s; \quad J_{10} = \int_0^1 \phi_2\psi''_{22}\mathrm{d}s;$$

$$J_{11} = \int_0^1 \phi_2\psi''_{1\bar{1}}\mathrm{d}s; \quad J_{12} = \int_0^1 \phi_2\psi''_{2\bar{2}}\mathrm{d}s; \quad J_{14} = \int_0^1 \phi'_1\psi'_{12}\mathrm{d}s$$

$$J_{15} = \int_0^1 \phi'_2\psi'_{22}\mathrm{d}s; \quad J_{16} = \int_0^1 \phi'_2\psi'_{1\bar{1}}\mathrm{d}s; \quad J_{17} = \int_0^1 \phi'_2\psi'_{2\bar{2}}\mathrm{d}s; \quad J_{18} = \int_0^1 \phi_2\psi_2\mathrm{d}s$$

and also

$$p^*_{22} = p_{22} + \frac{\alpha\beta I_1 I_{14}}{2\Omega^2\omega_1 I_{11}}; \quad p^*_{62} = p_{62} - \frac{\alpha\beta I_1 I_3}{4\Omega^2\omega_2 I_5}$$

Acknowledgements. This work was partially supported by a 2005 PRIN Grant financed by Italian Ministry of University (MIUR). Webpage: http://www.disg.uniroma1.it/fendis.

REFERENCES

Blevins, R. D., 1990, *Flow-induced Vibration*, 2nd edn, Van Nostrand Reinhold, New York.

Irvine, H. M., 1981, *Cable Structures*, The MIT Press, Cambridge, MA.

Lacarbonara, W., Paolone, A., and Vestroni, F., 2005, "Galloping instabilities of geometrically nonlinear nonshallow cables under steady wind flows," in *Proceedings of 2005 ASME Design Engineering Technical Conferences*, *DECT'05*, Long Beach, CA.

Lee, C. L. and Perkins, N. C., 1992, "Nonlinear oscillations of suspended cables containing a two-to-one internal resonance," *Nonlinear Dynamics* **3**, 465–490.

Luongo, A. and Piccardo, G., 1998, "Non-linear galloping of sagged cables in 1 : 2 internal resonance," *Journal of Sound and Vibration* **214(5)**, 915–940.

Luongo, A., Paolone, A., and Di Egidio, A., 2003, "Computational problems in multiple scale analysis," in *Recent Research Developments in Structural Dynamics*, A. Luongo (ed.), Research Signpost, India, pp. 1–31.

Luongo, A. and Piccardo, G., 2005, "Linear instability mechanisms for coupled translational galloping," *Journal of Sound and Vibration* **288(4-5)**, 1027–1047.

Luongo, A., Zulli, D., and Piccardo G., 2007, "A linear curved-beam model for the analysis of galloping in suspended cables," *Journal of Mechanics of Materials and Structures* **2(4)**, 675–694.

Martinelli, L. and Perotti, F., 2004, "Numerical analysis of the dynamic behavior of cables under turbulent wind," in *Proceedings of 2nd International Conference on Structural Engineering*, *SEMC 2004*, Cape Town, South Africa.

Novak, M., 1969, "Aeroelastic galloping of prismatic bodies," *Journal of the Engineering Mechanics Division*, ASCE **95(EM1)**, 115–142.

Pakdemirli, M., Nayfeh, S. A., and Nayfeh, A. H., 1995, "Analysis of one-to-one autoparametric resonances in cables – discretization vs. direct treatment," *Nonlinear Dynamics* **8**, 65–83.

Piccardo, G., 1993, “A methodology for the study of coupled aeroelastic phenomena,” *Journal of Wind Engineering and Industrial Aerodynamics* **48,** 241–252.

Rega, G., Lacarbonara, W., Nayfeh, A. H., and Chin, C. M., 1999, “Multiple resonances in suspended cables: direct versus reduced-order models,” *International Journal of Non-Linear Mechanics* **34**, 901–924.

Steindl, A. and Troger, H., 2001, “Methods for dimension reduction and their application in nonlinear dynamics,” *International Journal of Solids and Structures* **38,** 2131–2147.